Supplementary Information

Parameter	Value	References	Physical Meaning
p_ϕ	2x10^{-7} [1/h]	[1]	Physiologic collagen production
$p_{\phi,c}$	2x10^{-7} [1/h]	[2]	Collagen production activated by cytokine
$p_{\phi,J}$	2x10^{-7} [1/h]	[3]	Collagen production activated by stretch
$K_{\phi,c}$	0.0001 [-]	[3]	Saturation of cytokine effect in collagen production rate
$K_{\phi,\rho}$	1.06 [-]	[3]	Saturation of collagen production by collagen fraction
d_ϕ	0.00097 [1/h]	[1]	Collagen degradation
$d_{\phi,c}$	0.000485 [1/h]	[1]	Enhanced collagen degradation by collagen fraction
τ_ω	4.85 [h]	[3]	Time constant for reorientation
τ_κ	0.485 [h]	[3]	Time constant for dispersion
γ^κ	2 [-]	[3]	Shape of dispersion rate curve
$\tau_{\lambda_a^p}$	4.85x10^{-7} [h]	Estimated	Time constant for plastic deformation
$\tau_{\lambda_s^p}$	4.85x10^{-7} [h]	Estimated	Time constant for plastic deformation
$\tau_{\lambda_n^p}$	4.85x10^{-7} [h]	Estimated	Time constant for plastic deformation

Table 1: Parameters for the local extracellular matrix model. Parameters listed as estimated were selected in this work or modified from our previous wound healing model [3].

Parameter	Value	References	Physical Meaning
t_ρ	2x10^{-5} [MPa]	[4]	Traction
$t_{\rho,c}$	2x10^{-4} [MPa]	[3, 4]	Myofibroblast traction
$K_{t,c}$	0.0001 [-]	[3]	Traction saturation due to cytokine
K_t	0.4 [-]	Estimated	Traction saturation due to collagen
$D_{\rho\rho}$	0.0833 [mm^2/h]	[5, 6]	Cell diffusion coefficient
$D_{\rho c}$	1.66 x10^{-4} [mm^5/mol/h]	[2, 3]	Chemotaxis coefficient
D_{cc}	0.01208 [mm^2/h]	[2, 4, 7]	Cytokine diffusion coefficient
p_ρ	0.034 [1/h]	[5]	Cell proliferation
$p_{\rho,c}$	0.0085 [1/h]	Estimated	Cytokine-increased proliferation
$p_{\rho,J}$	0.0085 [1/h]	Estimated	Mechanoregulation of proliferation
$K_{\rho,c}$	0.0001 [-]	[3]	Proliferation saturation
d_ρ	$p_\rho(1-\rho_{phys}/K_{\rho\rho})$	[5]	Cell death rate
$K_{\rho\rho}$	0.0001 [cells/mm^3]	[5]	Cell division saturation
$p_{c,\rho}$	90e-16/10000 [1/h]	[3]	Cell secretion of cytokine
$p_{c,J}$	3e-18 [1/h]	[3]	Mechanoregulation of cytokine
$K_{c,c}$	1 [mol/mm^3]	[3]	Cytokine saturation
d_c	0.001 [1/h]	Estimated	Cytokine degradation
ρ_0	1000 [cells/mm^3]	[8, 9]	Dermal cell number
c_0	0.0001 [mol/mm^3]	[3]	Initial cytokine concentration
γ^{J^e}	5 [-]	[3]	Shape of mechanosensing curve
ϑ^e	2 [-]	[3, 10]	Midpoint of mechanosensing curve

Table 2: Parameters for the global biochemical and biomechanical model. Parameters listed as estimated were selected in this work or modified from our previous wound healing model [3].

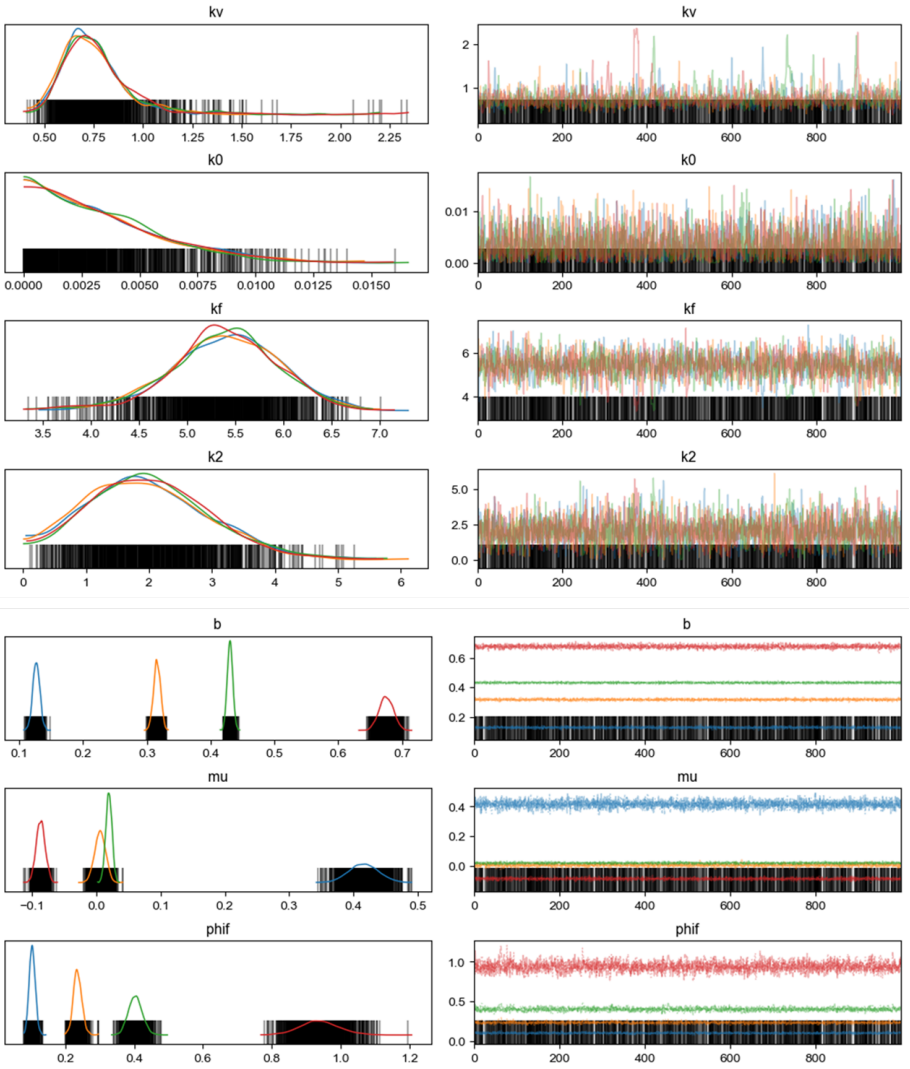

Figure 1: Trace plot of the Monte Carlo Markov Chain. Plots are shown for each of the shared (k_v, k_0, k_f, k_2) and unshared (b, μ, φ) parameters.

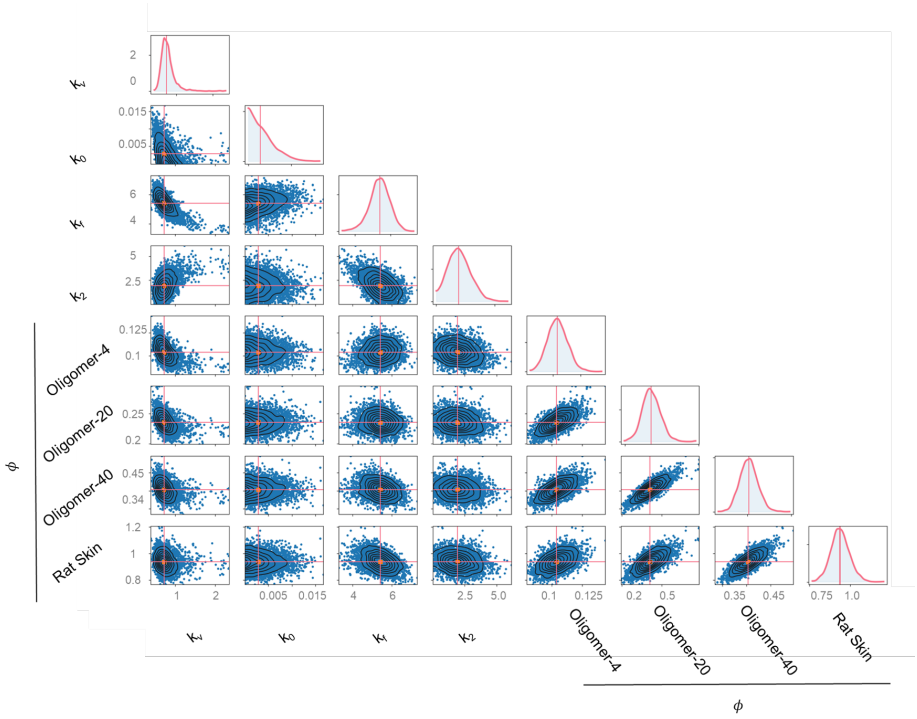

Figure 2: Pair plots of the stiffness parameters and collagen density for collagen scaffolds and rat skin. These parameters are directly linked together through the mechanical constitutive law and density measurements, and indirectly linked to the fiber orientation and dispersion. Covariance exists between k_v and other material parameters, as well as between the collagen Oligomer density measurements.

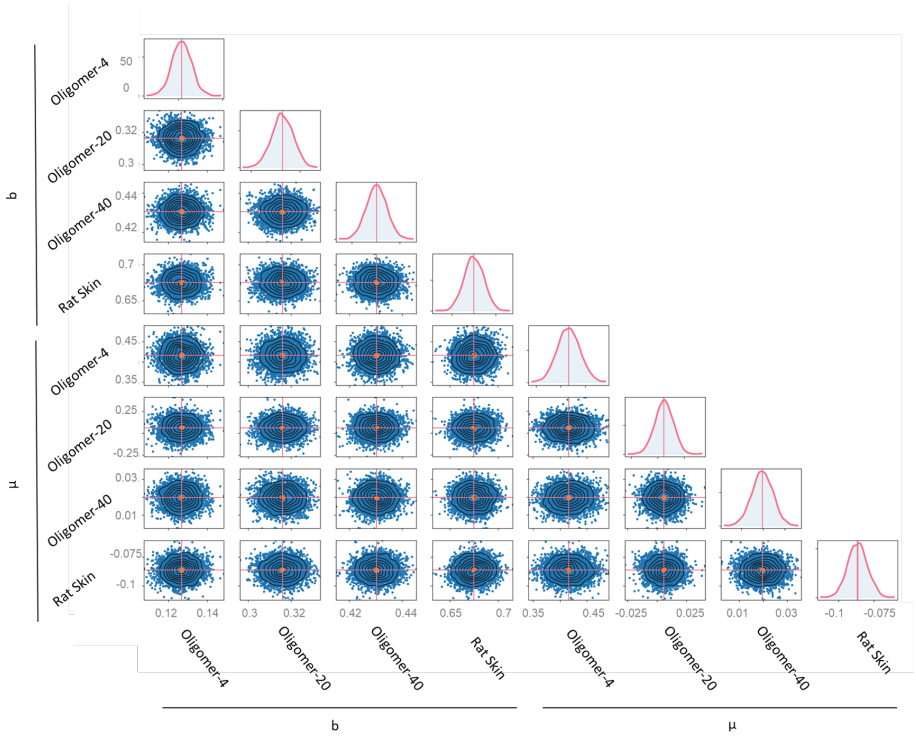

Figure 3: Pair plots of the fiber orientation and dispersion for collagen scaffolds and rat skin. These parameters are directly linked in the Von Mises fiber distribution and indirectly to the mechanical behavior. The plots suggest the parameters are largely independent.

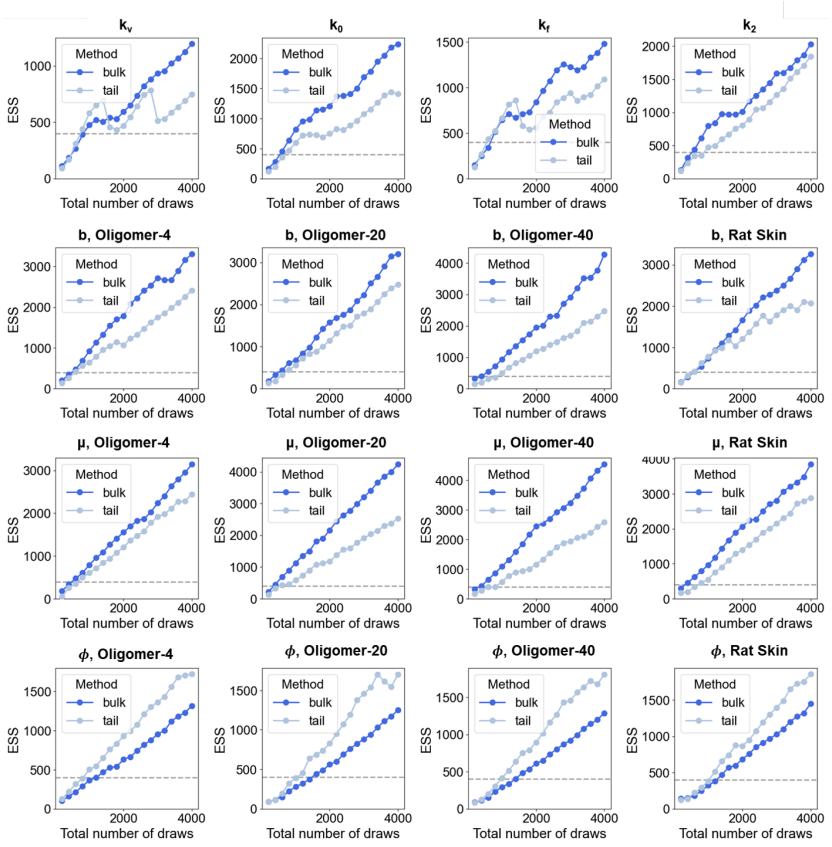

Figure 4: Evolution plot of the effective sample size. All parameters reach an ESS greater than 500, suggesting the chains have converged to their posterior value.

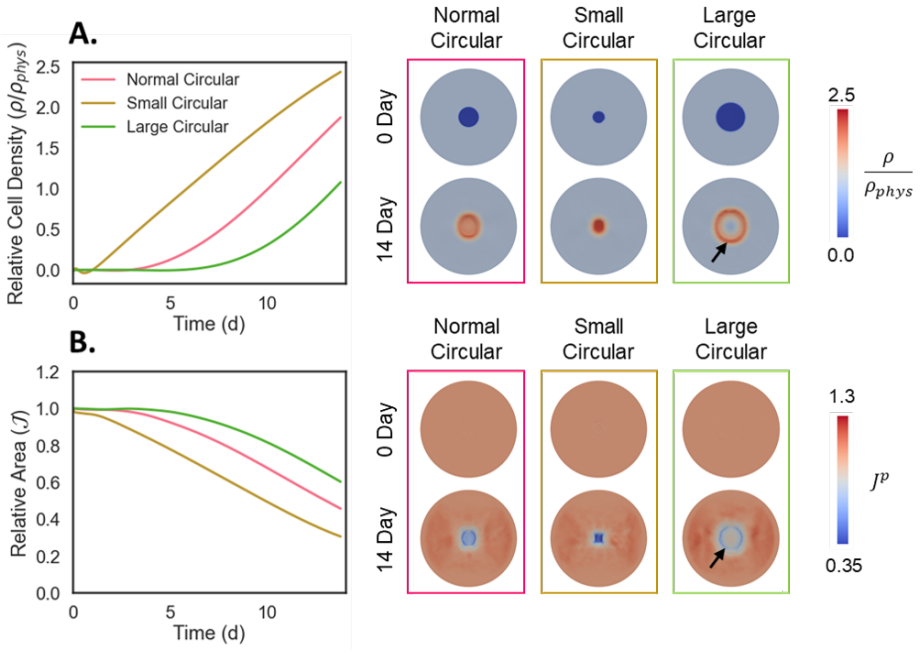

Figure 5: Effect of wound size on A. cellular infiltration in the wound center and B. contraction of isotropic Oligomer-40 treated wounds. Larger (2x) volume wounds undergo slower cellularization and contract moderately slower than smaller (1/2) volume wounds. This contraction is more evident at the wound border where the cells have successfully migrated.

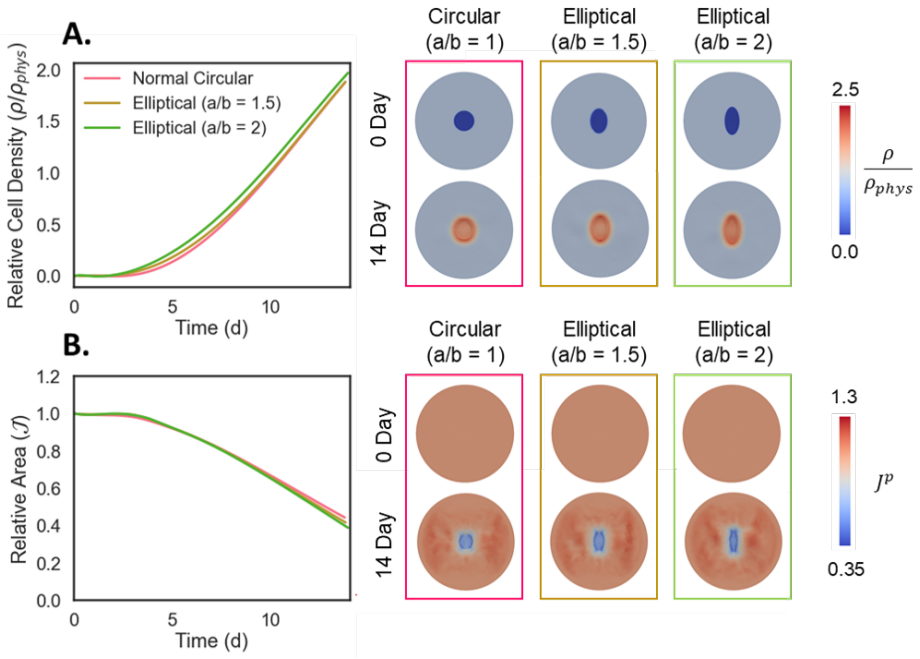

Figure 6: Effect of wound ellipticity on A. cellular infiltration in the wound center and B. contraction of isotropic Oligomer-40 treated wounds. Elliptical wounds have the same volume as circular wounds, but greater surface area at the interface between wound and surrounding skin tissue. The increase in surface area with ellipticity leads to somewhat faster recellularization and contraction, but to a small degree.

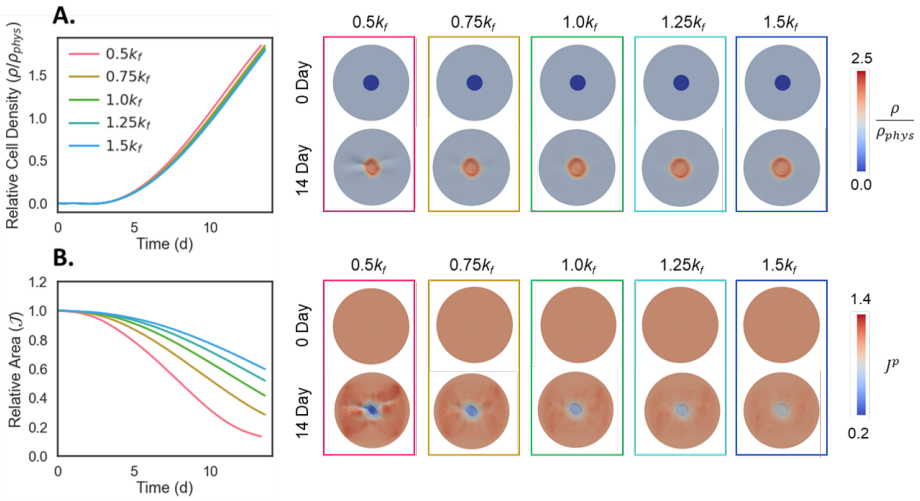

Figure 7: Effect of collagen stiffness on A. cellular infiltration in the wound center and B. contraction of isotropic Oligomer-40 treated wounds. Increasing collagen stiffness leads to significantly less contraction. Cellularization was not significantly affected by the change of collagen stiffness. This range of k_f is motivated in part by the possible uncertainty in material properties from the experimental setup, as well as inherent variability of material behavior of biological tissue. For example, uniaxial tests of murine, porcine, and human skin at different strain rates spanning three orders of magnitude have identified a relatively small change in the estimated modulus (1- to 3-fold change in estimated modulus) [11, 12, 13]. Note that all other parameters except k_f were kept constant and set to the values in Table S1.

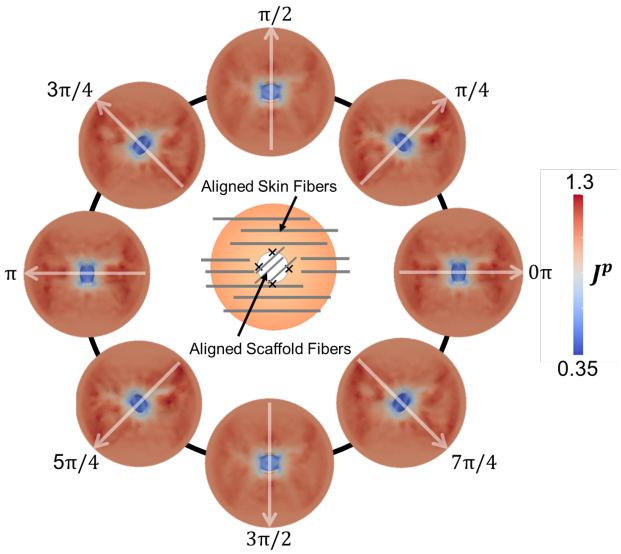

Figure 8: Effect of collagen scaffold fiber orientation on wound contraction. Skin fibers are maintained in a horizontal direction, $\mu_a = 0$ with alignment $\kappa = 0.2$ as in Figure 8, while collagen scaffold fibers are rotated from 0 to 2π. Due to the symmetry of the problem, after the first three cases, from 0 to $\pi/2$, the rest of the contours are equivalent to one of the first three cases. This shows that the code preserves these symmetries and that there are no mesh dependencies. As the scaffold fibers are rotated, the contracted wound shape rotates as well. This is due to the active stress term in eq. 11, which assumes that fibroblasts exert contractile forces primarily along the preferred fiber orientation with dispersion κ.

References

[1] G. Laurent, Dynamic state of collagen: pathways of collagen degradation in vivo and their possible role in regulation of collagen mass, American Journal of Physiology-Cell Physiology 252 (1) (1987) C1–C9.

[2] B. D. Cumming, D. McElwain, Z. Upton, A mathematical model of wound healing and subsequent scarring, Journal of The Royal Society Interface 7 (42) (2010) 19–34.

[3] A. Buganza Tepole, Computational systems mechanobiology of wound healing, Computer Methods in Applied Mechanics and Engineering 314 (2017) 46–70.

[4] D. C. Koppenol, F. J. Vermolen, F. B. Niessen, P. P. van Zuijlen, K. Vuik, A mathematical model for the simulation of the formation and the subsequent regression of hypertrophic scar tissue after dermal wounding, Biomechanics and Modeling in Mechanobiology 16 (1) (2017) 15–32.

[5] C. Valero, E. Javierre, J. M. García-Aznar, M. J. Gómez-Benito, A cell-regulatory mechanism involving feedback between contraction and tissue formation guides wound healing progression, PloS One 9 (3) (2014).

[6] K. Ghosh, Z. Pan, E. Guan, S. Ge, Y. Liu, T. Nakamura, X.-D. Ren, M. Rafailovich, R. A. Clark, Cell adaptation to a physiologically relevant ecm mimic with different viscoelastic properties, Biomaterials 28 (4) (2007) 671–679.

[7] K. E. Murphy, C. L. Hall, P. K. Maini, S. W. McCue, D. S. McElwain, A fibrocontractive mechanochemical model of dermal wound closure incorporating realistic growth factor kinetics, Bulletin of Mathematical Biology 74 (5) (2012) 1143–1170.

[8] C. Miller, G. Godeau, C. Lebreton-DeCoster, A. Desmouliere, B. Pellat, L. Dubertret, B. Coulomb, Validation of a morphometric method for evaluating fibroblast numbers in normal and pathologic tissues, Experimental Dermatology 12 (4) (2003) 403–411.

[9] E. Rognoni, A. O. Pisco, T. Hiratsuka, K. H. Sipilä, J. M. Belmonte, S. A. Mobasseri, C. Philippeos, R. Dilão, F. M. Watt, Fibroblast state switching orchestrates dermal maturation and wound healing, Molecular Systems Biology 14 (8) (2018) e8174.

[10] A. Buganza Tepole, C. J. Ploch, J. Wong, A. K. Gosain, E. Kuhl, Growing skin: A computational model for skin expansion in reconstructive surgery, Journal of the Mechanics and Physics of Solids 59 (10) (2011) 2177–2190.

[11] O. A. Shergold, N. A. Fleck, D. Radford, The uniaxial stress versus strain response of pig skin and silicone rubber at low and high strain rates, International Journal of Impact Engineering 32 (9) (2006) 1384–1402.

[12] M. Ottenio, D. Tran, A. N. Annaidh, M. D. Gilchrist, K. Bruyère, Strain rate and anisotropy effects on the tensile failure characteristics of human skin, Journal of the mechanical behavior of biomedical materials 41 (2015) 241–250.

[13] A. Pissarenko, W. Yang, H. Quan, K. A. Brown, A. Williams, W. G. Proud, M. A. Meyers, Tensile behavior and structural characterization of pig dermis, Acta biomaterialia 86 (2019) 77–95.